Robotica (2013) volume 31, pp. 371–379. © Cambridge University Press 2012
doi:10.1017/S0263574712000379

Precise outdoor localization with a GPS–INS integration system

Wonkyo Seo, Seoyoung Hwang, Jaehyun Park and Jang-Myung Lee*

School of Electrical Engineering, Pusan National University, Busan, South Korea

(Accepted July 2, 2012. First published online: July 26, 2012)

SUMMARY

This paper proposes a precise outdoor localization algorithm with the integration of Global Positioning System (GPS) and Inertial Navigation System (INS). To achieve precise outdoor localization, two schemes are recently proposed, which consist of de-noising the INS signals and fusing the GPS and INS data. To reduce the noise from the internal INS sensors, the discrete wavelet transform and variable threshold method are utilized, and to fuse the GPS and INS data while filtering out the noise caused by the acceleration, deceleration, and unexpected slips, the Unscented Particle Filter (UPF) is adopted. Conventional de-noising methods mainly employ a combination of low-pass and high-pass filters, which results in signal distortion. This newly proposed system also utilizes the vibration information of the actuator according to the fluctuations of the velocity to minimize the signal distortion. The UPF resolves the nonlinearities of the actuator and non-normal distributions of the noise more effectively than the conventional particle filter (PF) or Extended Kalman Filter–PF. The superiority of the proposed algorithm was verified through experiments, and the results are reported.

KEYWORDS: Robot localization; Mobile robots; Control of robotic systems; Motion planning; Navigation.

1. Introduction

Recently, precise localization schemes for outdoor navigation involving a combination of an Inertial Navigation System (INS) and a Global Positioning System (GPS) have been studied actively.[1–3] The INS is composed of an accelerometer, a gyroscope sensor, and a magnetic compass, which are used to estimate both position and velocity of the mobile robot. Even though the INS system provides precise location-information in a short time, the accumulative error caused additionally by the environmental disturbances is too big for it to be used for a long time. Note that the mobile robot motion on the irregular ground causes big accumulative errors by the change in velocities, friction to the ground, and vibrations of the mobile robot.

The GPS provides stable information on the absolute location. However, the GPS signal is very sensitive to the environment, which may block the signal path from satellites. Taking advantage of the two signals may provide the means to achieve precise localization in an outdoor environment.[4–7]

* Corresponding author. E-mail: jmlee@pusan.ac.kr

In conventional research, the filtering of the INS signals, which includes velocity-dependent noise, is performed using high-pass and low-pass filters. This scheme causes signal distortion, since it does not filter out the velocity-dependent noise effectively.[8] In the fusion of the INS and GPS signals, the Kalman Filter (KF) and the Extended Kalman Filter (EKF) are mostly utilized to obtain the position information, assuming that the motion characteristics of the mobile robot are linear, which results in a high-trajectory error for the mobile robot navigation.[9–12]

In this research, the Discrete Wavelet Transform (DWT) and the Variable Threshold Method (VTM) are utilized to actively filter out the velocity-dependent noise in the INS signals of a mobile robot, which are relatively free from signal distortion. Also, to propose a precise outdoor localization system for mobile robots, which has nonlinear and non-Gaussian noises, the Unscented Particle Filter (UPF), which has the advantages of the Particle Filter (PF) and Unscented Transform (UT), is used to fuse the INS and GPS signals.[13]

The main purpose of UPF in this paper is to compensate for the non-Gaussian characteristics of the GPS error and irregular motion characteristics of the mobile robot. The GPS error is coming from the time difference between the satellite and the mobile robot, geometrical difference among satellites, and multi-paths of the GPS signal. Also, the mobile robot receives and updates the GPS signal while it is moving on the ground, which causes the GPS error to be non-Gaussian.

This paper consists of six sections, including the Introduction. Section 2 describes the DWT/VTM used for the filtering of the acceleration data. The fusion of the INS and GPS signals is discussed in Section 3, and a precise outdoor localization scheme using the DWT/VTM and UPF is proposed in Section 4. Section 5 demonstrates the experimental results for the proposed precise localization algorithm. Finally, Section 6 concludes this research by proposing the future research.

2. Filtering of Acceleration Data

The INS signal is sensitive to the sensory white noise and external noise caused by the surface states and velocity of the mobile robot. The conventional approach using high-pass and/or low-pass filters is not effective in cancelling these noises and causes the accelerometer to be unreliable, since it is very susceptible to external shocks and vibrations.

2.1. Preliminary of Discrete Wavelet Transform

The DWT is a popular signal processing technique with Fast Fourier Transform (FFT) and Short-Time Fourier Transform

https://doi.org/10.1017/S0263574712000379 Published online by Cambridge University Press

(STFT). When the finite length basis function, $f(t)$, is defined to represent the original signal, it can be formed from the building blocks of the mother wavelet, $\psi(t)$.

The basic Wavelet Transform (WT) is represented as

$$f(t) = \sum_n a_n \psi_n(t). \tag{1}$$

The FFT is widely used for signal processing and solving differential equations. However, it cannot represent the time domain and frequency domain information at the same time. To overcome this shortcoming, the STFT, which has Fourier building blocks with a time-dependent weighting function, i.e., a window function, is introduced. Since the STFT uses an independent window function with the Fourier transform, its analysis is bounded to a certain time-frequency region and it is not efficient for the analysis of the non-stationary signals whose probabilistic characteristics are time-varying.

To avoid this problem, the WT scales the mother wavelet down or up to form suitable building blocks without using window functions as illustrated in Fig. 1. Therefore, it increases the resolution for signal analysis and provides an efficient time-frequency analysis compared with STFT.[14]

The DWT is a Multi Resolution Analysis (MRA), where the mother wavelet, $\psi(t)$, is shifted so as to have high scales at low frequencies and low scales at high frequencies. Its resolution can be adjusted to the desired level at the desired frequency.

The DWT is represented as

$$f = \sum_{j=-\infty}^{\infty} \sum_{k=-\infty}^{\infty} \langle f, \psi_{j,k} \rangle \psi_{j,k} \equiv \sum_{j=-\infty}^{\infty} \sum_{k=-\infty}^{\infty} d_j[k] \psi_{j,k}, \tag{2}$$

where f is represented by the wavelet only in $-\infty < t < \infty$ as the double summation of the scale index, j, and the horizontal displacement, k. $\langle f, \psi_{j,k} \rangle$ is the inner product of f and $\psi_{j,k}$. Using the MRA concept, $\psi(t)$ can be represented in terms of the scaling function, $\phi(t)$, as follows:

$$\psi(t) = \sqrt{2} \sum_n g_n \phi(2t - n), \tag{3}$$

where g_n is a high-pass filter. Also, the scaling function itself can be represented in terms of the scaling functions as,[15]

$$\phi(t) = \sqrt{2} \sum_n h_n \phi(2t - n), \tag{4}$$

where h_n is a low-pass filter. Note that there is a relation between the high-pass and low-pass filters, h_n and g_n:

$$g_n = (-1)^n h_{1-n}. \tag{5}$$

The upper level scaling function can be represented as the convolution of the scaling and wavelet functions of lower level. This implies that the lower frequency region in the first level can be decomposed into the higher and lower frequency regions in the second level. The decomposition is illustrated in Fig. 2.

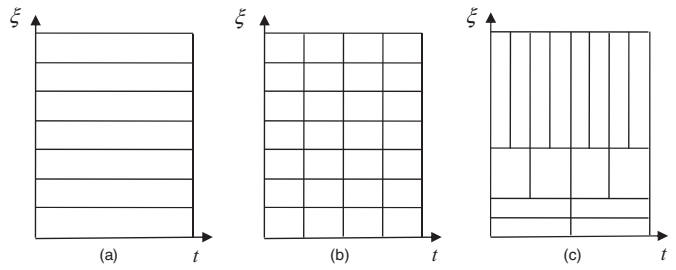


Fig. 1. Time-frequency analysis area by (a) Fourier transform; (b) short-time Fourier transform; (c) wavelet transform.

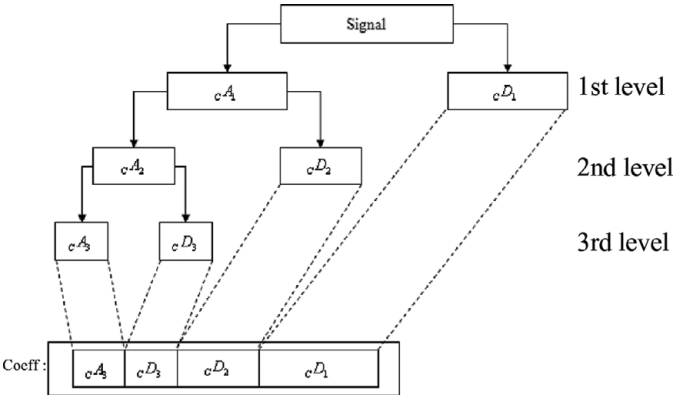


Fig. 2. Decomposition of multilevel 1D wavelet transform.

Figure 2 illustrates the process for multilevel 1D wavelet transform decomposition. Starting from a signal, two sets of coefficients are computed: approximation coefficients, ${}_cA_1$, and detail coefficients, ${}_cD_1$. These vectors are obtained by convolving with both low-pass filter h_n for approximation and high-pass filter g_n for detail, followed by dyadic decimation. The output decomposition structure contains the wavelet decomposition vector C.

2.2. *Filtering of noises in INS signal*

There are an acceleration sensor measuring the displacement and angle, a gyroscope sensor measuring the rotation angle, and a magnetic compass measuring the forwarding direction in the INS system, which is a major part of the localization system for the outdoor mobile robot. Among the sensors, the acceleration sensor is very sensitive to the robot motion. Therefore, in this research, it is proposed to filter out the motion-dependent noises using the DWT and VTM.

Figure 3 illustrates the noisy acceleration data, which are dependent on the velocity of the mobile robot.

2.3. *Variable Threshold Method*

To analyze the velocity-dependent signals, the DWT is adopted and the noises are filtered out by using the VTM. The VTM makes the wavelet coefficients of each level of the DWT converge to zero when the coefficients are below the threshold value. The VTM utilizes a soft threshold, T_λ^{soft},

https://doi.org/10.1017/S0263574712000379 Published online by Cambridge University Press

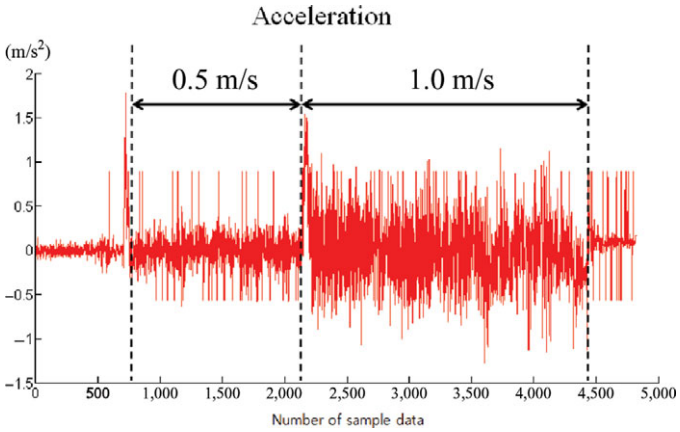


Fig. 3. (Colour online) Noise of acceleration signal due to actuator velocity variations.

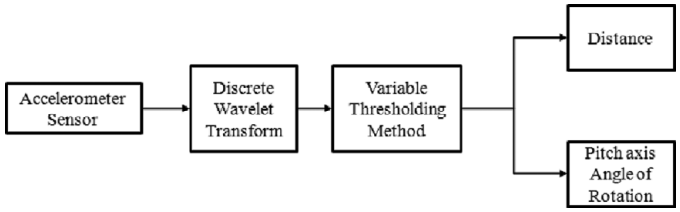


Fig. 4. De-noising of accelerometer sensor using DWT and VTM.

represented as

$$T_{\lambda}^{\text{soft}} = \begin{cases} u - \text{sign}(u)\lambda & \text{if } |u| \geq \lambda \\ 0 & \text{otherwise,} \end{cases} \tag{6}$$

where u represents the wavelet coefficients calculated by the DWT, and λ can be determined as

$$\lambda = \sqrt{2 \log n\sigma}, \tag{7}$$

where σ is the standard deviation of the signal, and n represents the number of samples.[16] Since λ is an important factor for the VTM performance in real situations, the optimal value of λ needs to be determined empirically. Since the DWT/VTM decomposes the velocity-dependent signals into the low- and high-frequency components and filters out the noises, the signal distortions can be minimized.

Figure 4 summarizes the de-noising process of the accelerometer data, which eventually provide the distance and angle values.

3. Fusion of GPS and INS Data

There have been several studies on solving dynamic systems to estimate state variables.[17] In the probabilistic approach, the probability space is formed by the state variables to estimate the state variables using its dynamic characteristics and measurements.[18] For the position estimation, the KF based on the Bayesian estimation and PF is widely used. In this research, GPS and INS are loosely integrated to simplify the system. To integrate and estimate the state variable in the dynamic system with high performance, the UPF, which is a combination of Unscented KF (UKF) and PF, is adopted in this research.

Table I. Typical filters for de-noising.

Filter	System model	Noise characteristics
KF	Linear	Normal distribution
Extended KF	Nonlinear	Normal distribution
Unscented KF (UKF)	Nonlinear	Normal distribution
PF	Nonlinear	Non-normal distribution

Particle Filter Algorithm

$[\{\mathbf{x}_k^i, \omega_k^i\}_{i=1}^N] = \mathbf{PF}[\{\mathbf{x}_{k-1}^i, \omega_{k-1}^i\}_{i=1}^N, \mathbf{z}_k]$

For $i = 1:N$

Sequential Important Sample (SIS)

- draw $\mathbf{x}_k^i \sim q(\mathbf{x}_k \mid \mathbf{x}_{k-1}^i, \mathbf{z}_k)$

- update weights $\omega_k^i = \omega_{k-1}^i \dfrac{p(\mathbf{z}_k \mid \mathbf{x}_k^i)p(\mathbf{x}_k^i \mid \mathbf{x}_{k-1}^i)}{q(\mathbf{x}_k \mid \mathbf{x}_{k-1}^i, \mathbf{z}_k)}$

END FOR

Calculate total weight $t = \text{SUM}[\{\omega_k^i\}_{i=1}^N]$

FOR $i = 1:N$

Normalize weights $\tilde{\omega}_k^i = t^{-1}\omega_k^i$

END FOR

If $N_{\text{eff}} < N_{\text{thr}}$,

Re-sample $[\mathbf{x}^i, \tilde{\omega}^i] \rightarrow [\mathbf{x}^j, N^{-1}]$

END IF

Fig. 5. The algorithm of particle filter.

3.1. Filter design

The typical filters for a given system model and given noise characteristics are summarized in Table I. The PF is suitable for processing nonlinear and non-Gaussian signals, since it uses probabilistic distribution for estimation.[19] The other filters are applicable under the assumption that the noises in the nonlinear systems are Gaussian.

The PF algorithm consists of Sequential Importance Sampling (SIS) and re-sampling. In the SIS process, the next particles are estimated with the weight for each particle. The distributions and weights for the ith particle of the kth states can be represented as given in refs. [20, 21]. Through the SIS process, the particles with low weights can be eliminated and the total number of particles is reduced. This may cause the nonefficient estimation of the particles. Therefore, the weights of the particles are equally redistributed through the resampling process to maintain the number of particles within a certain level.

The algorithm of PF is illustrated in Fig. 5,[22] and the progress of PF is schematically shown in Fig. 6.

After process of SIS and re-sampling, the particle and weight are used to estimate the next state, $\hat{\mathbf{x}}_k$, as

$$\hat{\mathbf{x}}_k = \sum_{i=1}^{N} \tilde{\omega}_k^i f(\mathbf{x}_k^i), \tag{8}$$

where f represents the system function.

https://doi.org/10.1017/S0263574712000379 Published online by Cambridge University Press

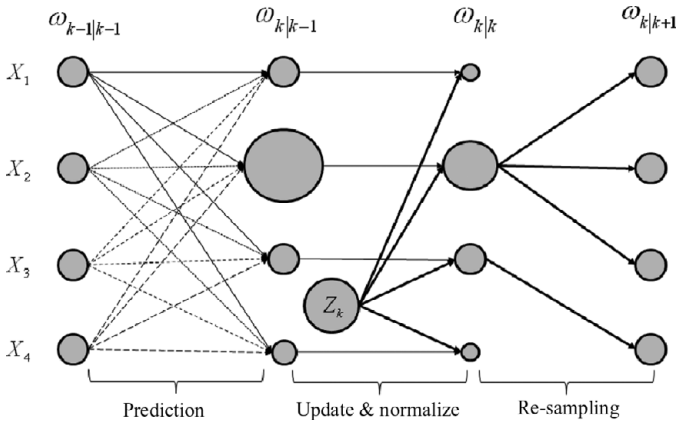


Fig. 6. Progress of particle filter.

The average and covariance are estimated and propagated precisely in the SIS process when the UKF is utilized for the nonlinear system. Therefore, the UPF propagates the average and covariance using the UT. The UT determines the sample points for random variables of the average $\bar{\mathbf{x}}$ (L-dimension) and covariance $\mathbf{P}_X$. The sample points are determined as follows:

$$\boldsymbol{\chi}_i = \begin{cases} \bar{\mathbf{x}} + \sqrt{(L+\lambda)\mathbf{P}_{\mathbf{x}}}\big|_i, & \text{when } i = 1, \ldots, L, \\ \bar{\mathbf{x}} - \sqrt{(L+\lambda)\mathbf{P}_{\mathbf{x}}}\big|_{i-L}, & \text{when } i = L+1, \ldots, 2L. \end{cases} \tag{9}$$

Note that $\boldsymbol{\chi}_0 = \bar{\mathbf{x}}$, and $\sqrt{(L+\lambda)\mathbf{P}_x}\big|_i$ implies the ith column of the matrix square root. The scaling parameter, λ, is defined as

$$\lambda = \alpha^2(L+\kappa) - L. \tag{10}$$

The constant α determines the spread of the sigma points around $\bar{\mathbf{x}}$, and is usually set to a small positive value (e.g., $10^{-4} \leq \alpha \leq 1$). The constant κ is a secondary scaling parameter, which is usually set to $3 - L$.

To determine the mean of sigma points, weights, $W^{(m)}$, are determined as follows:

$$W_i^{(m)} = \begin{cases} \dfrac{\lambda}{(L+\lambda)}, & \text{when } i = 0, \\ \dfrac{1}{2(L+\lambda)}, & \text{for } \quad i = 1, \ldots, 2L. \end{cases} \tag{11}$$

Therefore, the mean of the sample points, $\bar{\mathbf{x}}^i_{k|k-1}$, is represented as

$$\bar{\mathbf{x}}^i_{k|k-1} = \sum_{j=0}^{2L} W_j^m f\left(\boldsymbol{\chi}^i_{j,k|k-1}\right). \tag{12}$$

To obtain the covariance of sigma points, the weights, $W^{(c)}$, are determined as follows:

$$W_i^{(c)} = \begin{cases} \dfrac{\lambda}{(L+\lambda)} + 1 - \alpha^2 + \beta, & \text{when } i = 0, \\ \dfrac{1}{2(L+\lambda)}, & \text{for } \quad i = 1, \ldots, 2L, \end{cases} \tag{13}$$

where β is used to incorporate prior knowledge of the distribution of $\mathbf{x}$ (for Gaussian distributions, $\beta = 2$ is optimal).[23]

Now the covariance of the sample points, $\mathbf{P}^i_{k-1}$, is represented as

$$\mathbf{P}^i_{k-1} = \sum_{j=0}^{2L} W_j^c \left(\boldsymbol{\chi}^i_{j,k|k-1} - \bar{\mathbf{x}}^i_{j,k|k-1}\right)\left(\boldsymbol{\chi}^i_{j,k|k-1} - \bar{\mathbf{x}}^i_{j,k|k-1}\right)^T. \tag{14}$$

The Kalman gains, $\mathbf{K}$, can be obtained by the covariance of measured values, $\mathbf{P}_{\mathbf{zz}}$, and the covariance of estimated and measured values, $\mathbf{P}_{\mathbf{xz}}$, with the concept of UT as follows:

$$\mathbf{K}_k = \mathbf{P}_{\mathbf{x}_k z_k} \mathbf{P}_{\tilde{\mathbf{z}}_k \tilde{\mathbf{z}}_k}. \tag{15}$$

The Kalman gains, $\mathbf{K}$, obtained in Eq. (15) can be used to estimate the average $\bar{\mathbf{x}}_k$ as

$$\bar{\mathbf{x}}^i_k = \bar{\mathbf{x}}^i_{k|k-1} + \mathbf{K}_k\left(\mathbf{z}_k - h\left(\bar{\mathbf{x}}^i_{k|k-1}\right)\right), \tag{16}$$

where h represents the measurement function.

The covariance $\mathbf{P}_k$ is represented as

$$\mathbf{P}^i_k = \mathbf{P}^i_{k|k-1} - \mathbf{K}_k \mathbf{P}_{\tilde{\mathbf{z}}_k \tilde{\mathbf{z}}_k} \mathbf{K}_k^T. \tag{17}$$

Equation (17) defines the UPF, which improves the accuracy of the PF through the computation of the average and covariance determining the next particle distribution of the SIS using the UT concept. The application of the UT concept to SIS can be represented as

$$\mathbf{x}^i_k \sim q\left(\mathbf{x}^i_k | \mathbf{x}^i_{0:k-1}, \mathbf{z}^k_0\right) \approx N\left(\bar{\mathbf{x}}^i_k, \mathbf{P}^i_k\right), \tag{18}$$

where z^k_0 is the measured value obtained from GPS, and q represents the probability of the SIS process.

The advantage of UKF over EKF to approximate the proposal distribution lies in the fact that UKF can better handle the heavy-tailed distributions, thus is more tailored for non-Gaussian scenarios. In fact, UPF has been successfully applied in object-tracking, robot navigation. Both EKF proposal and UKF use Gaussian approximation of proposal, but UKF produces more accurate estimate than EKF and it is derivative-free.[24]

3.2. Fusion of INS and GPS

The UPF-based fusion modeling of INS and GPS for the outdoor localization system can be represented as a block diagram, which is a combination of UKF and PF.

https://doi.org/10.1017/S0263574712000379 Published online by Cambridge University Press

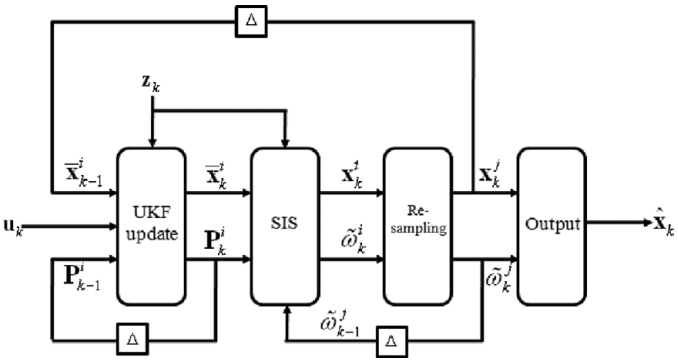


Fig. 7. UPF-based fusion model of INS and GPS.

The UPF-based system can estimate the states more precisely than the general PF, since it utilizes UKF as shown in Fig. 7, which is suitable for nonlinear and nonstandard-deviation systems. The fusion model of the UPF input $\mathbf{u}_k$ is composed of the three axes acceleration data (A_x), pitch angle from the gyroscope sensor (G_p), and yaw angle from the gyroscope sensor (G_y). State $X_k$is composed of the (x_k, y_k) position, velocity (v_k), pitch angle (θ_k), and yaw angle (ψ_k) values. The measurement values $\mathbf{z}_k$ are obtained from the National Marine Electronics Association (NMEA) code of GPS, and these are transformed into the (x_k, y_k) position. The pitch angle is obtained based upon the acceleration data (θ_k), and the yaw angle is obtained based upon the magnetic compass (ψ_k). Therefore, the UPF was modeled with the components derived above($\mathbf{u}_k$, $\mathbf{x}_k$, $\mathbf{z}_k$).

The measuring system can be represented generally in the state space as follows:

$$\dot{\mathbf{x}}_k = f(\mathbf{x}_{k-1}, \mathbf{u}_{k-1}, \mathbf{w}_{k-1}), \tag{19}$$

$$\mathbf{z}_k = \mathbf{H}\mathbf{x}_k + \mathbf{v}_k, \tag{20}$$

where $\mathbf{x}_k = [x_k \;\; y_k \;\; v_k \;\; \theta_k \;\; \psi_k]^T$, $\mathbf{u}_k = [A_{x,k} \;\; G_{p,k} \;\; G_{y,k}]^T$, $\mathbf{w}_k = [w_{x,k} \; w_{y,k} \; w_{v,k} \; w_{\theta,k} \; w_{\psi,k}]^T$, $\mathbf{v}_k = [v_{x,k} v_{y,k} v_{\theta,k} v_{\psi,k}]^T$, and $\mathbf{z}_k = [\, x_k \;\; y_k \;\; \theta_k \;\; \psi_k \,]^T$.

Note that $\mathbf{w}_k$ and $\mathbf{v}_k$ are the system and the measuring noises respectively, and these are not assumed to be Gaussian to represent the real system closely.

The GPS/INS system in this research is modeled as follows:

$$\dot{x}_k = v_{k-1}\cos(\psi_{k-1}) + \mathbf{w}_{k-1}(1), \tag{21a}$$

$$\dot{y}_k = v_{k-1}\sin(\psi_{k-1}) + \mathbf{w}_{k-1}(2), \tag{21b}$$

$$\dot{v}_k = A_x\cos(\theta_{k-1}) + \mathbf{w}_{k-1}(3), \tag{21c}$$

$$\dot{\theta}_k = G_p + \mathbf{w}_{k-1}(4) = \mathbf{u}_{k-1}(2) + \mathbf{w}_{k-1}(4), \quad \text{and} \tag{21d}$$

$$\dot{\psi}_k = G_y + \mathbf{w}_{k-1}(5). \tag{21e}$$

The linear measurement model is represented as

$$\mathbf{z}_k = \begin{bmatrix} 1 & 0 & 0 & 0 & 0 \\ 0 & 1 & 0 & 0 & 0 \\ 0 & 0 & 0 & 1 & 0 \\ 0 & 0 & 0 & 0 & 1 \end{bmatrix} \mathbf{x}_k + \mathbf{v}_k. \tag{22}$$

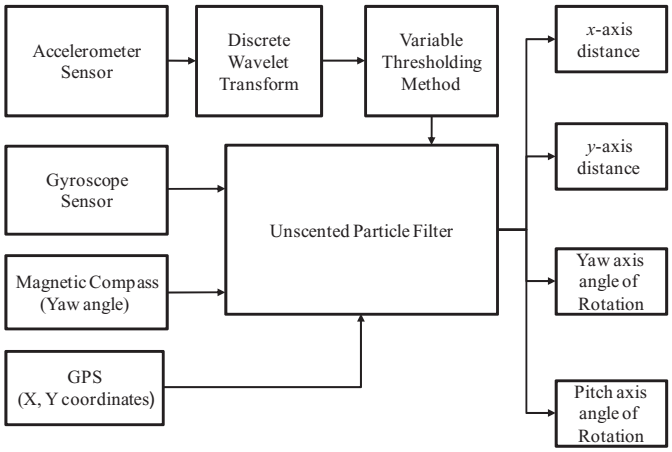


Fig. 8. Block diagram of precise outdoor localization.

The GPS data are updated every 1 s and the fusion of the INS and GPS data provides accurate position information every 0.01 s for the outdoor mobile robot. Each particle of the UPF gets the acceleration data as input and integrates the values to estimate the next states, which are obtained from the angular velocities of pitch and yaw axis based upon the gyroscope sensor data. The UT is utilized in this step to propagate the next states precisely for the nonlinear system.

The pitch angle based upon the accelerometer, yaw angle from the magnetic compass, and (x, y) position based upon the GPS data are used as the measurement model to update the weight for each particle when the GPS data are updated every 1 s. Note that the weight for each particle is inversely proportional to the displacement from the measurement values. The modified yaw and pitch angles and the (x, y) position of the robot can be obtained by summing the weights for the particles.

4. Precise Localization System for Outdoor Navigation

4.1. Experimental environment

In this research, we attempt to minimize the distortion of the signal when the velocity-dependent INS noises are filtered out. To achieve this, the DWT and the velocity-dependent VTM are utilized. Also, a precise outdoor localization system for a mobile robot is proposed, which uses the UPF to fuse the INS and GPS data. The acceleration data passed through the DWT and VTM processes are used to estimate the displacement of a mobile robot and to compensate for the accumulative error of the gyroscope sensor on the pitch axis. The magnetic compass is used to compensate for the gyroscope sensor error on the yaw axis.

Figure 8 illustrates the outdoor localization system for a mobile robot. The velocity, distance, and the orientation of a mobile robot are obtained in the UPF block using the gyroscope, accelerometer, magnetic compass, and the GPS data.

4.2. Hardware construction

The INS used for this research is composed of a three-axes accelerometer, two one-axis gyroscope sensors, and

https://doi.org/10.1017/S0263574712000379 Published online by Cambridge University Press

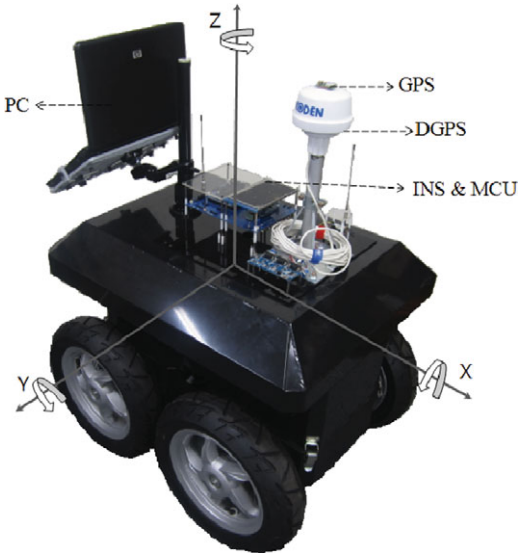


Fig. 9. (Colour online) Precise outdoor location estimation system and outdoor moving robot.

a magnetic compass with the TI TMS320F28335 MCU. The three-axes accelerometer is SCA3000-D01 ($\pm$ 2 g) made by VTI technologies Corporation, the gyroscope sensor is ADIS6100 ($\pm$ 300^o/s) from Analog Devices, the magnetic compass is designed using the KMZ10A of Philips Corp., and the GPS is a UIGGUB02-R001 of UI_GOODS Corporation. For the calibration of the acceleration sensor, the measured data at six stationary positions are utilized. The off-set value for the gyroscope sensor has been compensated by using the average bias value for 10 s.[25]

The outdoor mobile robot has four 300 W DC motors with encoders. The physical size of the mobile robot is 732 (W) $\times$ 920 (H) $\times$720 (D) mm. The accelerometer is aligned to the x-axis, that is, the forward motion direction of the mobile robot as shown in Fig. 9. The gyroscope sensors are placed for the yaw and pitch axes, and the magnetic compass is set up for the yaw axis. The university playground is selected as the experimental environment, since its surface is relatively flat and there are not many obstacles against navigation.

The DGPS KBG-3 of KODEN Corporation is used as the reference system for the localization system. The slippage and time-accumulative errors of encoders are not compensated for the precise mobile robot navigation and for the evaluation of the GPS–INS integration system.

5. Experiments and Results

Straight-line and curved paths are selected for the experimental environments. For each environment, the 30-m path is divided into three 10-m slots, and the speed is set to 0.47 m/s at the first slot, 1.00 m/s at the second slot, and 1.26 m/s at the last slot for the navigation of the mobile robot.

Figures 10(a)–(c) illustrate the acceleration, velocity, and distance along the x-axis in the straight-line motion respectively. The results are obtained from the acceleration sensor data along the x-axis for 37 s, giving about

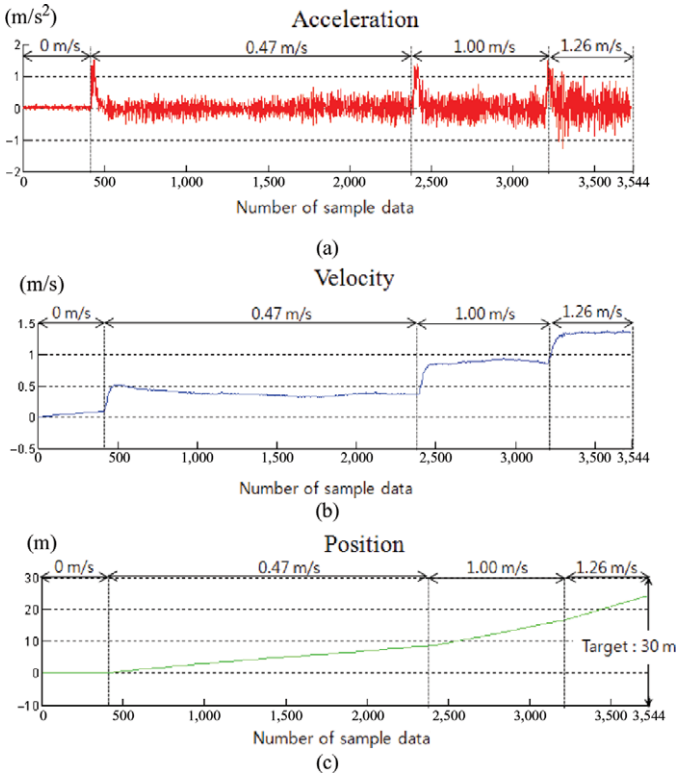


Fig. 10. (Colour online) (a) Acceleration along x-axis in the straight-line motion; (b) velocity of x-axis in the straight movement; (c) distance of x-axis in the straight movement.

3,744 sensor data every 0.01 $\sim$ 0.011 s, without using the DWT/VTM. Because of high-frequency components in the signal, the velocity is slightly increased while the mobile robot is stationary, as shown in Fig. 10(b). As shown in Fig. 10(c), the travel distance along the x-axis has an error of $-$5.8 m at the final location because of the disturbances and accumulative errors during navigation.

To eliminate the noises in the acceleration sensor adaptively, the Discrete approximation of Meyer wavelet (Dmey), which is a family of wavelets, is adopted. For the decomposition, the level 5 DWT is used for signal analysis, and the results of the VTM applications are compared with the original signals.

As shown in Fig. 11(a)–(c), the noises in the acceleration signal are eliminated, and the traveling distance error is reduced to less than –2 m at the final location. The de-noising effect of the DWT/VTM is compared with the KF, which is the most popular scheme for data estimation.

As shown in Fig. 12, the original acceleration sensor data include an error of about $-$5.8 m, which is reduced to $-$4.13 m by the KF and to –1.97 m by the DWT/VTM. This clearly represents the superiority of the DWT/VTM for the de-noising of the acceleration data.

The processed acceleration data, gyroscope data of the INS, and magnetic compass data are fused with the National Electronic Association's (NMEA) GPRMC code of GPS using the UPF, and are used for estimating the navigation trajectories of the outdoor mobile robot.

Table II summarizes the coefficients of UPF, system noises, and measurement noises.

https://doi.org/10.1017/S0263574712000379 Published online by Cambridge University Press

Table II. UPF coefficients.

Parameter		Coefficient
Number of particle		$N = 100$
Number of valid particle		$N\text{th} = 0.8\ N$
System noise	Gyro sensor (yaw, pitch)	$\pm 0.1^{o}/s$
	Acceleration sensor (x, y, z)	$\pm 0.1\ m/s^2$
Measurement noises	GPS	± 3 m
	Magnetic compass (yaw)	± 2.5
	Acceleration sensor (pitch)	$\pm 5^{o}$

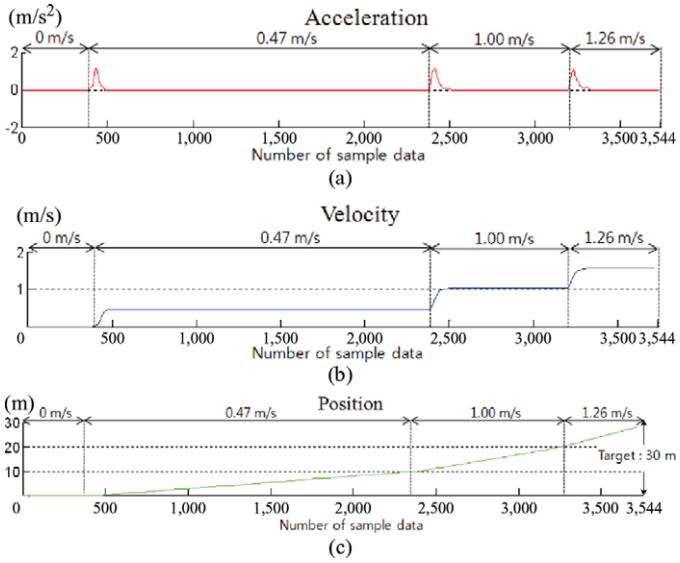


Fig. 11. (Colour online) (a) Acceleration of x-axis in the straight movement after DWT and VTM; (b) velocity of x-axis in the straight movement after DWT and VTM; (c) distance of x-axis in the straight movement after DWT and VTM.

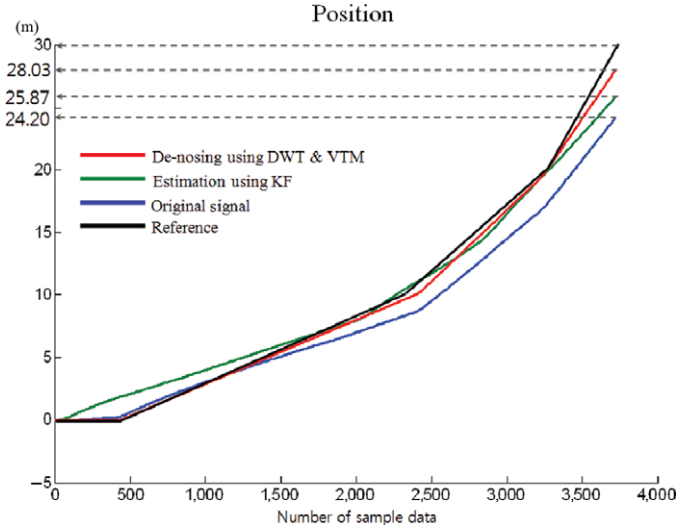


Fig. 12. (Colour online) Performance comparison of DWT & VTM with KF.

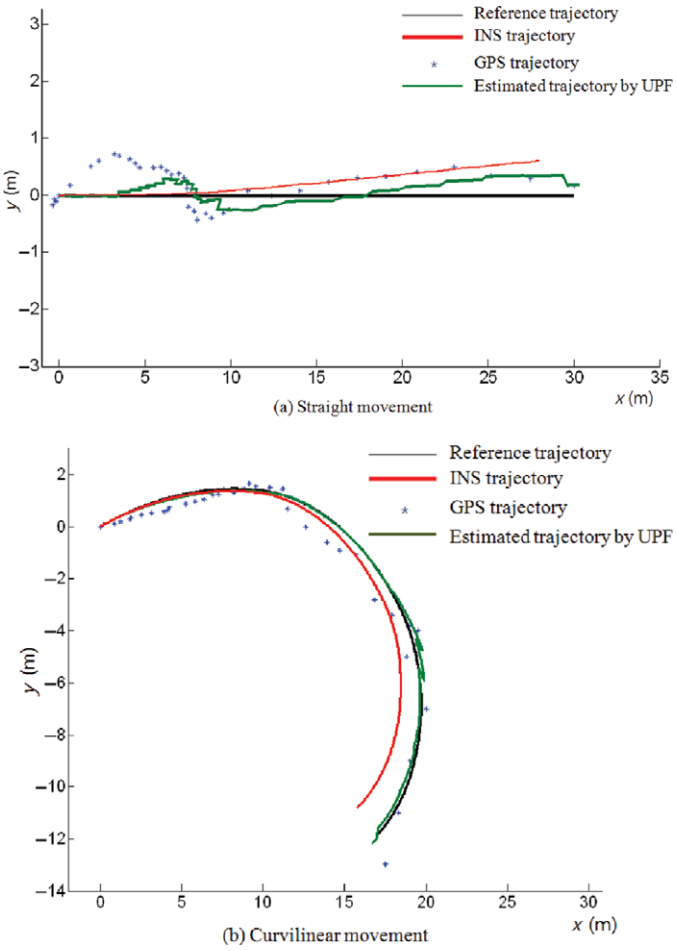


Fig. 13. (Colour online) Location estimation consequence of INS/GPS integration using UPF.

Straight-line and curved trajectories are selected for a mobile robot to evaluate the estimation performance of the proposed scheme in fusing the GPS and INS data.

In Fig. 13, the trajectory errors for the straight and curved lines are illustrated. The deviation of the INS trajectory from the reference trajectory increases with time. This comes from the accumulative error of the gyroscopic sensor for estimating the yaw-axis angle. The localization error using the GPS signals is about ± 3 m without any obstacles to the receipt of the signal. The trajectory estimated by the proposed algorithm is very close to the reference trajectory, where the INS signals and the GPS data are fused by the UPF to compensate for each other's shortages in real time.

The performance of the UPF in estimating the trajectory by the fusion of the INS and GPS data is compared with those of the EKF–PF and UKF in Fig. 14. It is clearly recognized that the UPF provides the closest estimation to the reference among three algorithms.

Table III compares the mean error and standard deviation of the EKF–PF, UKF, and UPF in the straight-line motion, where the UPF has the smallest error.

Table IV compares the mean error and standard deviation of the EKF–PF, UKF, and UPF in the curved-line motion, where the UPF has the smallest error.

Tables V and VI illustrate the performance of EKF–PF, UKF, and UPF in detail for 10 times of the tracking of

https://doi.org/10.1017/S0263574712000379 Published online by Cambridge University Press

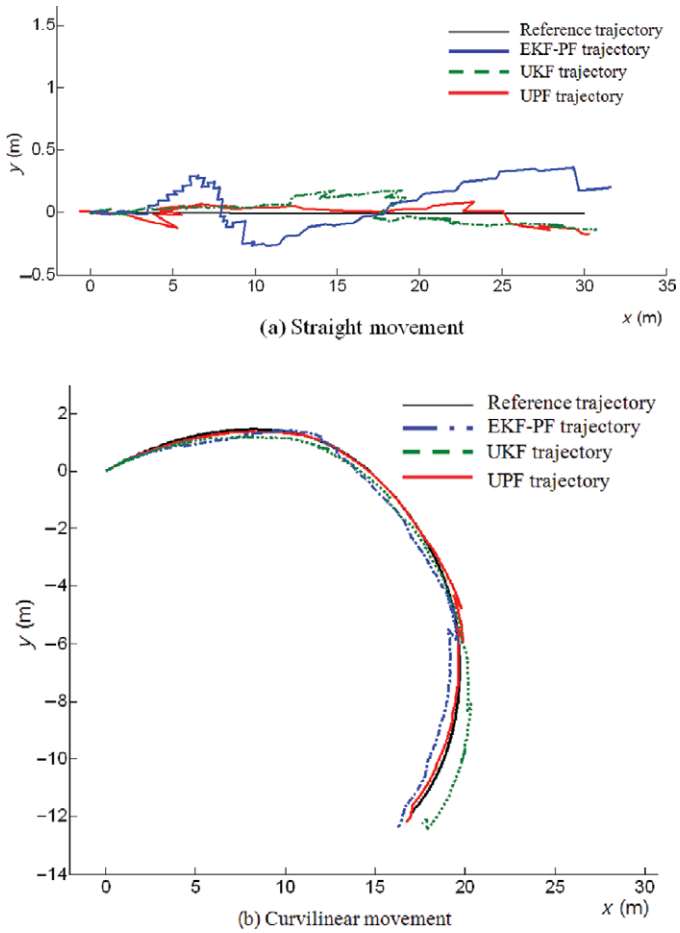


Fig. 14. (Colour online) Performance comparison results of EKF–PF, UKF, and UPF.

Table III. Performance comparison of EKF–PF, UKF, and UPF in the straight-line motion.

Error \ Filter	EKF–PF	UKF	UPF
Mean error (m)	0.195	0.156	0.122
Standard deviation (m)	0.077	0.058	0.040

Table IV. Performance comparison of EKF–PF, UKF, and UPF in curvilinear movement.

Error \ Filter	EKF–PF	UKF	UPF
Mean error (m)	0.586	0.581	0.578
Standard deviation (m)	0.444	0.438	0.426

the straight and curved line trajectories by the mobile robot respectively.

6. Discussion and Future Research

It is very difficult to properly handle the noises of INS sensors for the precise localization of mobile robots, since the motion of the mobile robot is nonlinear and the noises are not Gaussian. Therefore, linear and Gaussian approximations are required to form a real-time system. There is no algorithm that satisfactorily overcomes these difficulties in a reasonable manner, although there have been many studies on this subject. In this paper, the noises in the signal of the accelerometer composing the INS from the motion of the mobile robot are efficiently removed using the DWT and

Table V. Performance comparison of EKF–PF, UKF, and UPF in the straight-line motion.

Trial #	Error \ Filter	EKF–PF	UKF	UPF
1	Mean error (m)	0.217	0.149	0.124
	Standard deviation (m)	0.081	0.053	0.043
2	Mean error (m)	0.201	0.146	0.127
	Standard deviation (m)	0.076	0.054	0.042
3	Mean error (m)	0.205	0.145	0.126
	Standard deviation (m)	0.081	0.061	0.047
4	Mean error (m)	0.2.03	0.155	0.117
	Standard deviation (m)	0.082	0.054	0.035
5	Mean error (m)	0.209	0.152	0.124
	Standard deviation (m)	0.087	0.059	0.043
6	Mean error (m)	0.199	0.153	0.118
	Standard deviation (m)	0.078	0.045	0.041
7	Mean error (m)	0.207	0.159	0.131
	Standard deviation (m)	0.074	0.054	0.042
8	Mean error (m)	0.205	0.154	0.122
	Standard deviation (m)	0.085	0.051	0.041
9	Mean error (m)	0.193	0.156	0.127
	Standard deviation (m)	0.068	0.048	0.033
10	Mean error (m)	0.195	0.158	0.125
	Standard deviation (m)	0.073	0.058	0.043
Average	Mean error (m)	0.203	0.153	0.124
	Standard deviation (m)	0.079	0.054	0.041

Table VI. Performance comparison of EKF–PF, UKF, and UPF in curvilinear movement.

Trial #	Error \ Filter	EKF–PF	UKF	UPF
1	Mean error (m)	0.595	0.578	0.569
	Standard deviation (m)	0.445	0.434	0.431
2	Mean error (m)	0.583	0.577	0.570
	Standard deviation (m)	0.446	0.435	0.419
3	Mean error (m)	0.577	0.578	0.571
	Standard deviation (m)	0.448	0.446	0.432
4	Mean error (m)	0.598	0.576	0.571
	Standard deviation (m)	0.432	0.424	0.421
5	Mean error (m)	0.582	0.580	0.572
	Standard deviation (m)	0.445	0.447	0.428
6	Mean error (m)	0.579	0.578	0.569
	Standard deviation (m)	0.442	0.441	0.431
7	Mean error (m)	0.582	0.574	0.566
	Standard deviation (m)	0.452	0.427	0.429
8	Mean error (m)	0.576	0.581	0.575
	Standard deviation (m)	0.449	0.433	0.433
9	Mean error (m)	0.573	0.578	0.564
	Standard deviation (m)	0.447	0.434	0.425
10	Mean error (m)	0.611	0.581	0.573
	Standard deviation (m)	0.451	0.445	0.427
Average	Mean error (m)	0.585	0.578	0.570
	Standard deviation (m)	0.445	0.436	0.427

https://doi.org/10.1017/S0263574712000379 Published online by Cambridge University Press

VTM. Also, it is proposed that the nonlinear motion of the mobile robot and the non-Gaussian noises of INS and GPS can be harmonically combined through the UPF. The application of laser range finders to reduce the localization error for the autonomous navigation of a mobile robot in an unstructured environment is left as a future research project.

Acknowledgments

This work was supported (in part Pusan National University Specialized Navigation/Localization Robot Technology Research Center) by the Ministry of Knowledge Economy under Human Resources Development Program for Convergence Robot Specialists.

References

1. A. Soloviev and F. van Graas, "Enhancement of integrated GPS/INS performance utilizing frequency domain implementation of INS calibration," *J. Inst. Navig.* **54**(2) (2007, Feb.).
2. H. Liu, S. Nassar and N. E. Sheimy, "Two-filter smoothing for accurate INS/GPS land-vehicle navigation in urban centers," *IEEE Trans. Veh. Technol.* **59**(9), 4256–4267 (2010).
3. S. Han and J. Wang, "Land vehicle navigation with the integration of GPS and reduced INS: Performance improvement with velocity aiding," *Robotica* **63**(1), 153–166 (2010).
4. S. Kim, C. Roh, S. Kang and M. Park, "Outdoor Navigation of a Mobile Robot Using Differential GPS and Curb Detection," **In**: *Proceedings of the 2007 IEEE International Conference on Robotics and Automation*, Roma, Italy (Apr. 10–14, 2007) pp. 3414–3419.
5. G. T. Schmidt, *INS/GPS Technology Trends* (NATO Research and Technology Organization, France, May 2009).
6. V. Di. Lecce, A. Amato and M. Calabrese, "GPS-Aided Lightweight Architecture to Support Multi-Sensor Data Synchronization," **In**: *Proceedings of 2008 IEEE Instrumentation and Measurement Technology Conference (IMTC 2008)*, Canada (2008) pp. 149–154.
7. P. D. Groves, R. J. Handley and A. R. Runnalls, "Optimising the integration of terrain referenced navigation with INS and GPS," *Robotica* **59**(1), 71–89 (2006).
8. L. Gang, Y. Jie, W. Lixin, G. Jiang and W. Xiaomei, "Detecting and Extracting Vibration Disturb in IMU Testing in Field", **In**: *Proceedings of the 2nd International Conference on Computer Engineering and Technology (ICCET)*, Chengdu, China (2010) pp. V2516–V2518.
9. H. H. Dong, H. X. Lin, L. M. Ming and S. Z. Yue, "Federated unscented particle filtering algorithm for SINS/CNS/GPS system," *J. Central South Univ. Technol.* **17**(4), 778–785 (2010).
10. J. Yi, H. Wang, J. Zhang, D. Song, S. Jayasuriya and J. Liu, "Kinematic modeling and analysis of skid-steered mobile robots with applications to low-cost inertial-measurement-unit-based motion estimation," *IEEE Trans. Robot. on* **25**(5), 1087–1097 (2009).
11. S. Baselga, L. G. Asenjo, P. Garrigues and J. L. Lerma, "Inertial navigation system data filtering prior to GPS/INS integration," *Robotica* **62**(4), 711–720 (2009).
12. J. Zhou, S. Knedlik and O. Loffeld, "INS/GPS tightly coupled integration using adaptive unscented particle filter," *Robotica* **63**(3), 491–511 (2010).
13. J. K. Lee and C. Jekeli, "Rao-blackwellized unscented particle filter for a handheld unexploded ordnance geolocation system using IMU/GPS," *Robotica* **64**(2), 327–340 (2011).
14. P. Barralon, N. Vuillerme and N. Noury, "Walk Detection With a Kinematic Sensor: Frequency and Wavelet Comparison," **In**: *Proceedings of the IEEE 2006 International Conference of the Engineering in Medicine and Biology Society (EMBS '06),* New York, USA (2006) pp. 1711–1714.
15. R. K. Young, *Wavelet Theory and Its Applications* (Kluwer, the Netherlands, 1993).
16. A. K. Chan and C. Peng, *Wavelets for Sensing Technologies* (Artech, London, 2003).
17. S. M. Rock, J. D. Powell and P. Enge, Design and Performance of a Robust GPS/INS Attitude System for Automobile Application (*Ph.D. Dissertation* (Stanford University, Stanford, CA, 2004).
18. B. Ristic, S. Arulampalam and N. Gordon, *Beyond the Kalman Filter* (Artech, London, 2004).
19. J. K. Lee, D. J. Cacamise II, C. Jekeli, "The Precise INS/GPS Geolocation of a Vehicle-Towed UXO Detection System," **In**: *Proceedings of the Position Location and Navigation Symposium (PLANS, 2010) IEEE/ION*, South Carolina (2010) pp. 1189–1195.
20. L. Tian, J. Rong, X. Zhong and T. Li, "UPF Algorithm and its Application in the GPS/INS Integrated Navigation," **In**: *Proceedings of International Conference on Wireless Communications & Signal Processing, 2009 (WCSP 2009)*, Nanjing, China (2009) pp. 1–4.
21. S. Yang, Q. Ma and W. Huang, "Particle Swarm Optimized Unscented Particle Filter for Target Tracking," **In**: *Proceedings of the 2nd International Congress on Image and Signal Processing, 2009 (CISP '09)*, Tianjin, China (2009) pp. 1–5.
22. M. S. Arulampalam, S. Maskell, N. Gordon and T. Clapp, "A tutorial on particle filters for online nonlinear/non-gaussian bayesian tracking," *IEEE Trans. Signal Process.* **50**(2), 174–188 (2002).
23. S. Haykin, *Kalman Filtering and Neural Networks* (Wiley, Colorado, 2001) pp. 228–229.
24. Z. Chen, "Bayesian Filtering: From Kalman Filters to Particle Filters and Beyond," *Technical Report* (Adaptive Systems Laboratory, McMaster University, Hamilton, Ontario, Canada, 2003) 38 pp.
25. Z. F. Syed, P. Aggarwal, C. Goodall, X. Niu and N. El-Sheimy, "A new multi-position calibration method for MEMS inertial navigation systems," *Meas. Sci. Technol.* **18**, 1897–1907 (2007).

https://doi.org/10.1017/S0263574712000379 Published online by Cambridge University Press